Available online at www.sciencedirect.com
ScienceDirect
International Journal of Heat and Fluid Flow 29 (2008) 927–944
International Journal of HEAT AND FLUID FLOW
www.elsevier.com/locate/ijhff

Experimental approach and numerical prediction of a turbulent wall jet over a backward facing step

N. Nait Bouda [a,*], R. Schiestel [b], M. Amielh [b], C. Rey [c], T. Benabid [a]

[a] LMFTA, Faculté de Physique, Université de Sciences et Technologie Houari Boumediène, Bab Ezzouar, 16111 Alger, Algeria
[b] IRPHE, UMR 6594, CNRS-Universités d'Aix-Marseille, Technopôle de Château-Gombert, 49 rue F. Joliot Curie, 13384 Marseille Cedex 13, France
[c] MSNM-GP-L3M, UMR 6181, CNRS Institut Méditerranéen de Technologie, Technopôle de Château-Gombert, 38 rue F. Joliot-Curie, 13451 Marseille Cedex 20, France

Received 31 May 2007; received in revised form 12 December 2007; accepted 8 January 2008
Available online 4 March 2008

Abstract

The process of separation and reattachment in a turbulent wall jet flow over a backward facing step is studied both experimentally and numerically. On the experimental point of view, laser Doppler anemometry is implemented to provide an overall understanding of the particular flow features of this turbulent flow. The incoming wall jet presents a particular structure with two different sources of turbulence production (the first one located in the inner shear layer is due to near wall velocity gradients with small scale eddies and the second one corresponds to the free shear jet-like flow in the external region with entrainment by large turbulence scales). So the present study, including experimental and numerical points of view, gives new insights into the role of these large eddies in the outer flow and their interaction with the near wall region and the recirculation zone. Numerically, the computational results are obtained by solving the two-dimensional Reynolds Averaged Navier–Stokes (RANS) equations. The approach is based on one point statistical modelling using a low Reynolds number second order full stress transport closure, derived from the Launder and Tselepidakis model (1991) and coupled to a two-scale energy-flux model (RSMKFL2).

Keywords: Backward facing step flow; Turbulence modelling; Wall jet flow; Second moment closure

1. Introduction

Separation is a phenomenon which appears under a variety of flow conditions and encountered in many engineering problems. The performance of fluid machinery in industrial flows is greatly influenced by its occurrence. So, to control flow separation, many investigations by numerous authors have been conducted in fluids engineering. A widely known case is the backward facing step flow. Indeed it provides an excellent test flow for studying the basic physical phenomena of separation and reattachment. This geometry is of particular interest because separation is imposed at the step edge and one can focus attention on the study of reattachment process, while in many real engineering flows separation and reattachment are interacting and then occurring at variable distances. The backward facing step (BFS) flow has been extensively studied, but many aspects of the flow structure and the dynamics of this geometrically simple turbulent flow remain incompletely explained.

The principal flow features of turbulent BFS flow are described as follows: a turbulent boundary layer of thickness δ, which develops on a flat plate, encounters a backward facing step of height h. The sudden change in surface geometry causes the boundary layer to separate at the sharp step edge. The resulting flow behaves downstream, essentially like a free shear layer, with high speed flow on the upper side and low speed flow on the lower

* Corresponding author. Tel.: +213 21 24 79 60.
E-mail address: n.naitbouda@yahoo.fr (N. Nait Bouda).

0142-727X/$ - see front matter © 2008 Elsevier Inc. All rights reserved.
doi:10.1016/j.ijheatfluidflow.2008.01.002

Notation

Roman symbols

b	nozzle height
C_f	skin friction coefficient, $C_f = 2\frac{\tau_w}{\rho U_{max}^2}$
l	nozzle width
h	step height
p	static pressure at the wall
p_0	static pressure at the reference section $x = -10h$
$R_{ij} = \overline{u_i u_j}$	kinematic Reynolds stress
$Re_h = \frac{U_0 h}{\nu}$	Reynolds number based on h
u_i	velocity fluctuation
u', v', w'	Cartesian components of rms fluctuating velocity
U_0	maximum streamwise velocity at $x = -15h$
x, y, z	coordinate system
X_r	reattachment length
T_u	turbulence intensity $\sqrt{\overline{u'2}}/\bar{u}$
τ_w	wall shear stress

Greek symbols

δ_{ij}	Kronecker delta
ε	kinematic dissipation rate of k
$\tilde{\varepsilon}$	homogeneous part of dissipation rate of k
ε_{ij}	dissipation rate of R_{ij}
ν	kinematic viscosity
ν_t	turbulent viscosity
ρ	fluid density

side. Some distance downstream, the shear layer impinges on the surface and then forms a closed recirculation region containing turbulent, moving fluid. A small counter-rotating "corner eddy" developing below the mean recirculating bubble flow may also exist in this region. The instantaneous location of reattachment occurs over a region located all around the time averaged reattachment point X_r and it is found to vary slightly in time about its mean position. Downstream of reattachment, the boundary layer begins to redevelop undergoing a relaxation towards a standard turbulent boundary layer state (Fig. 2).

Some of the earlier studies have been focused on understanding the parameters which affect the reattachment process in this flow from the point of view of the suppression and control of the separation process. Other studies put a major emphasis on observation and analysis of such a flow field. The effect of the Reynolds number, as one of the important parameters, has been studied by Eaton and Johnston (1980) and Durst and Tropea (1981). The effect of the ratio of boundary layer thickness to the step height was clarified by Le Huu Nho (1994). The effect of streamline curvature on the reattachment length was examined in the experiments in curved channels (Honami and Kakajo, 1986). An extensive study on the expansion ratio E_r in a channel (E_r defined as the ratio of the test section height downstream of the step to the upstream height) was made by Durst and Tropea (1981) and Ra and Chang (1990). The aspect ratio (width to height ratio) was furthermore examined by De Brederode and Bradshaw (1972), and the effect of inlet turbulence intensity was considered by Isomoto and Honami (1989) and also the wall roughness by Badri Kusuma (1993).

Eaton and Johnston (1980), Adams and Johnston (1988) and Driver and Seegmiller (1985) measured the skin friction coefficient C_f on the step wall, all of whom reported high values of C_f in the recirculation region. Later, Jovic and Driver (1994, 1995) and Le et al. (1997) showed that the peak value in C_f can be significantly higher at low Reynolds numbers.

Some early attempts at flow control were made by Chun and Sung (1996), Sigurdon (1995) and more recently by Shuya et al. (2001). They studied the periodic perturbation (alternating suction and injection) effect on the turbulent reattaching flow. Their results revealed essentially the existence of an optimum frequency range for promoting reattachment. Under such conditions, the reattachment length extended to only half its standard reference length.

Up to now, no systematic and extensive study has been made about the influence of external turbulence structure on the step flow. On this purpose, the aim of the present work is precisely to get new informations on the influence of the external flow on the recirculation region and particularly on its spatial extension. The incoming flow considered in the present case is a wall jet. We shall show that considering a wall jet instead of a standard boundary layer, may considerably modify the flow structure in the wall region of the step. In a jet flow, the outer free shear layer induces mass entrainment of fluid and the free boundary is characterized by the presence of large eddies. In a previous experimental work Nait Bouda et al. (2005) emphasize the role of big eddies on the recirculation zone downstream of a backward facing step. These large eddies interact with the separated recirculating zone and promote the flapping of the impingement of the jet on the wall, making the reattachment point to fluctuate and simultaneously the mean reattachment length to decrease.

The phenomena observed in the present flow after a backward facing step is also encountered in many industrial processes involving fluid separation. For instance, these phenomena may occur at the entrance of a semi-permeable membrane in filtering devices or in cyclone separation systems. In environmental applications, the wind acceleration over hills generates wall jet-type flows and then similar mechanisms are found in the formation of

snow-drifts, the displacement of dunes and the silting of rivers. The study of more academic configurations in a laboratory model is thus of particular interest for the understanding and the control of these phenomena. Furthermore, the turbulent wall jet is a basic flow of fundamental interest for turbulence research because of its two-fold characteristics (Launder and Rodi, 1981, 1983; Wygnanski et al., 1992). The inner layer of the plane wall jet is similar to a classical turbulent boundary layer while the outer layer is like a free jet. Consequently, the turbulent wall jet presents two major sources of turbulence production: one of them is located in the inner wall shear layer and characterized by small scale eddies, and the other pertains to the free jet outer region of the flow characterized by strong entrainment of fluid by large eddies. The external turbulent large eddies produce real changes in the dynamics of the flow over a backward facing step. One of the important properties to look at is the reattachment length, because it indicates the rate of mixing in the separated shear layer which is very sensitive to the incoming flow parameters cited above.

The numerical approach of BFS flows have also received significant attention, we can cite for instance the work of Lien and Leschziner (1994), Le et al. (1997), Hanjalic and Jakirlic (1998) and Kang and Choi (2002).

The turbulent backward facing step flow is an excellent test case for the validation of turbulence models. This same flow includes three typical zones of different types: a separated shear layer when the incoming jet reaches the step edge, a recirculating flow region extending down to the stagnation point followed by a relaxation region. These different regions are often used to test the validity and the degree of universality of one point statistical turbulence closures which have been tuned against simple academic homogeneous and non homogeneous flows.

When the flow separates, a curved and highly turbulent free shear layer is formed first. In this layer, the turbulence anisotropy can have a much greater influence on mean flow characteristics than the one of the parent boundary layer (or wall jet). This is due, mainly, to the strong interaction between curvature, strain and normal stresses on the one hand and to the sensitivity of the shear layer to normal stress anisotropy on the other hand. The importance of anisotropy entails a strong appeal for using second moment closures in the modelling of separated and recirculating flows. Numerous studies have given ample evidence for the predictive superiority of second moment closure over eddy viscosity models in a significant number of complex flows and with respect to various flow features. However, several studies have also put in light some drawbacks (Obi et al., 1991; Lasher and Taulbee, 1990). It was found that excessive levels of anisotropy and physically unrealistic reattachment process appear as the main weaknesses of usual second moment closures (Launder et al., 1975; Gibson and Launder, 1978). Since then, efforts were made to cure some of the aforementioned defects (Lien and Leschziner, 1994; Craft and Launder, 1996; Craft, 1998; Hanjalic and Jakirlic, 1998) by introducing more advanced closure hypotheses. In these models, the main turbulence interactions are represented by individual source terms and among them the normal stress anisotropy production. In the present work, we have used a hybrid multiple scale model with partial energies coupled to an extension of the Launder and Tselepidakis second order full stress transport closure. Indeed, the present flow may present departures from standard equilibrium state and it was interesting to include some possibilities to account for possible spectral effects and non equilibrium.

Thus, the present numerical investigation is based on the solution of the Reynolds averaged Navier–Stokes equations using second moment closure. The complexity of turbulence interactions, in particular the important role played by the anisotropy has been the argument for choosing a Reynolds Stress Transport Model. In addition, the two time scale energy model is coupled to the Reynolds stress equations in order to account for departures from equilibrium. A low turbulence Reynolds number extension of these models has been used in order to describe accurately the viscous sublayer at the wall.

2. Experimental setup and measurements

2.1. Test section

A wind tunnel initially developed for free jet studies has been modified to carry on wall jet investigations. The experimental test rig is essentially composed of three parts, shown in Fig. 1. The first part consists in a convergent channel (2) ended by a 40 mm high (b) and 700 mm wide (ℓ) nozzle. The second part (5) is the inlet region, located upstream the step and measuring about 1100 mm long (L) and 700 mm wide (ℓ). Then, the third part corresponds to the backward facing step, with a step height $h = 20$ mm, followed by the recirculating flow region. Thus, the experimental configuration corresponds to typical turbulent "separation and reattachment" phenomena (Adams et al., 1984).

The experimental rig was limited laterally by plane parallel walls. One of the side walls is made of plexiglass, as well as the bottom wall. Using plexiglass for the bottom wall is suitable for improving near wall LDA measurements since the smoothness and transparency of the material minimise the diffusive surface reflections (Johnson and Brown, 1990). The vertical plexiglass wall allows both to make flow visualizations and to perform the LDA measurements in the xOy plane. The reference mean velocity is defined as the maximum velocity measured at the $x/h = -15$ cross section upstream of the step and is equal to $U_0 = 5.8$ m/s for $y = y_{max}$. The resulting Reynolds number based on the step height is $Re_h = 7600$. At the same cross section $x/h = -15$, the turbulence intensity in the main flow is about 13%.

The inner boundary layer thickness at the edge of the step is about $\delta \approx 20$ mm. In such a case for which $\delta/h \cong 1$, the free shear mixing layer is affected by the

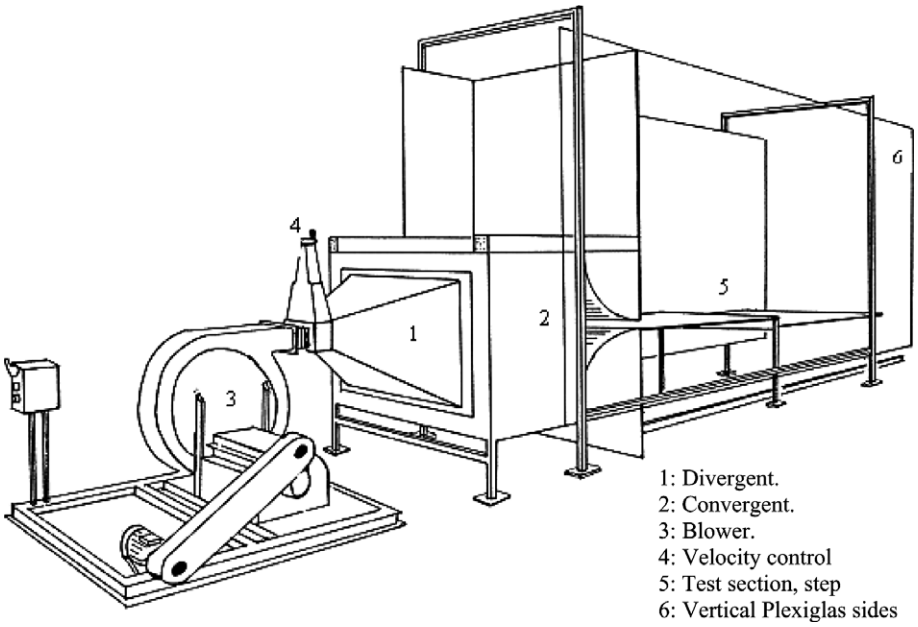

Fig. 1. Experimental set up.

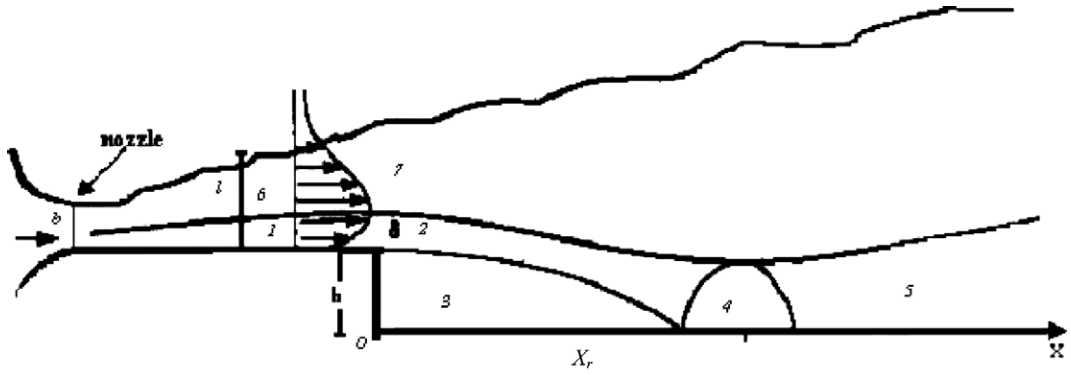

Fig. 2. Schematic pattern of flow structure.

upstream flow but not dominated by it (Bradshaw and Wong, 1972).

In the present experimental study the aspect ratio of the backward facing step is $l/h = 35$, a sufficiently large value to ensure practically the two-dimensionality of the flow according to the criteria of De Brederode and Bradshaw (1972).

The inlet flow configuration, notation and coordinate system used in the present work are summarized in Fig. 3, the z-coordinate pertains to the spanwise direction. The inner region is defined as the region extending from the wall itself up to the point located at a wall distance y_{max} where the mean velocity is maximum $U_{max} = U(y_{max})$. The outer region is located beyond y_{max} i.e. for $y > y_{max}$.

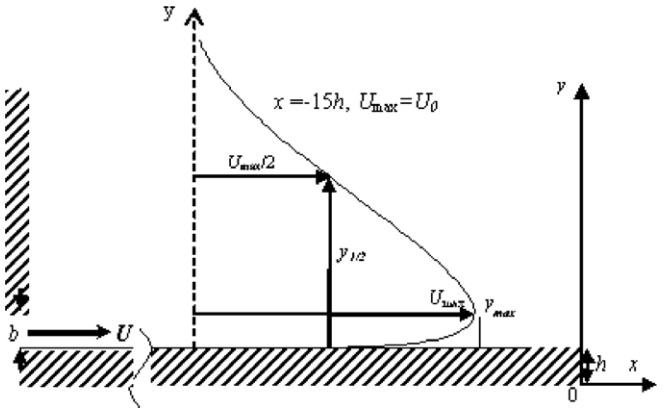

Fig. 3. Configuration and nomenclature for the plane wall jet.

A preliminary study of the flow in the recirculating and reattachment zones was already done by Badri Kusuma et al. (1992). The visualization system used by these authors is described in this previous paper. Their investigation was complemented by hot wire anemometry (HW) measurements (Badri Kusuma, 1993). For measurements in the recirculating zone, a specific probe was designed. This probe described by Badri Kusuma (1993) consists of two parallel wires mounted to lay in the same plane at a separation distance of 0.1 mm. The first one (the hot wire) operates at constant temperature for measuring the instantaneous velocity. The second one (the cold wire) located downstream, operates at constant current and gives information on the velocity vector direction: when the cold wire is located in the thermal wake of the hot wire, the velocity is positive otherwise the velocity is negative. Nevertheless, the use of hot wire technique in recirculating zones remains controversial and is indeed often inadequate.

In the present investigation, the measurements were carried on using laser Doppler anemometry with the aim to compare and complement the hot wire measurements which remain questionable in the recirculation zone.

2.2. Laser Doppler anemometer system

A 2D laser Doppler anemometer (DANTEC) was used to measure the two orthogonal components of velocity. The system consists in a continuous laser source (Argon-ion type with 2 W emitting power), a transmitting optical device (beam splitter and focusing lens) and a receiving optical device (photodetectors PM55X08 and PM57X08). In addition, a Bragg cell was used in order to distinguish between negative and positive flow velocities. The beam splitter generates three laser beams (blue, green, blue + - green) with two different wavelengths (blue = 488 nm, green = 514.5 nm) that allow simultaneous data acquisition of the two velocity components.

Depending on the area under investigation, two different lenses were mounted. For the measurement in the transverse plane (xOz), the optical probe head is installed inside the wind tunnel and a lens with a 160 mm focal length is used. Then, the size of the probe volume is $0.078 \times 0.078 \times 0.93\ \text{mm}^3$ for the streamwise velocity component, and $0.074 \times 0.074 \times 0.88\ \text{mm}^3$ for the spanwise velocity component. For the measurement in the normal plane (xOy), the optical probe head is located outside of the wind tunnel. In order to reach the centerline of the test section, we used a lens with a 399 mm focal length. The size of the probe volume is then larger, namely $0.19 \times 0.19 \times 5.8\ \text{mm}^3$ (streamwise velocity component) and $0.18 \times 0.18 \times 5.5\ \text{mm}^3$ (normal velocity component).

The receiving optics was mounted on a mechanism allowing the displacement of the measurement volume with a one millimeter step. So, the first measurement point reached near the wall is located at $y \cong 2$ mm from the wall.

Using the LDA system in air requires the introduction of seeding materials to serve as scattering particles. For this, we used a "Jem Techno Haze Performance" type smoke generator located directly at the inlet of the blower. So, the interactions of the seeder with the flow field were minimized and the blower itself could help to distribute the seeds uniformly. The smoke was generated by pumping a thin film of "pro haze fluid" into the heating engine and then the vaporized oil was condensing in the air stream into seed particles.

According to the technique proposed by Le Huu Nho (1994) for detecting at least the minimal number of points that are necessary to ensure a good statistical treatment, the acquisition time was chosen greater than 40 s and generally more than 2000 points at every location are acquired via the AT interface board which is controlled by the Floware software (Dantec). Using the same considerations, Adams and Eaton (1988) estimated the statistical uncertainty at less than 1%. On the other hand, these authors pointed out that velocity bias is significant in highly turbulent regions.

One of the most usual methods for correcting the bias errors is based on the residence time of the particles in

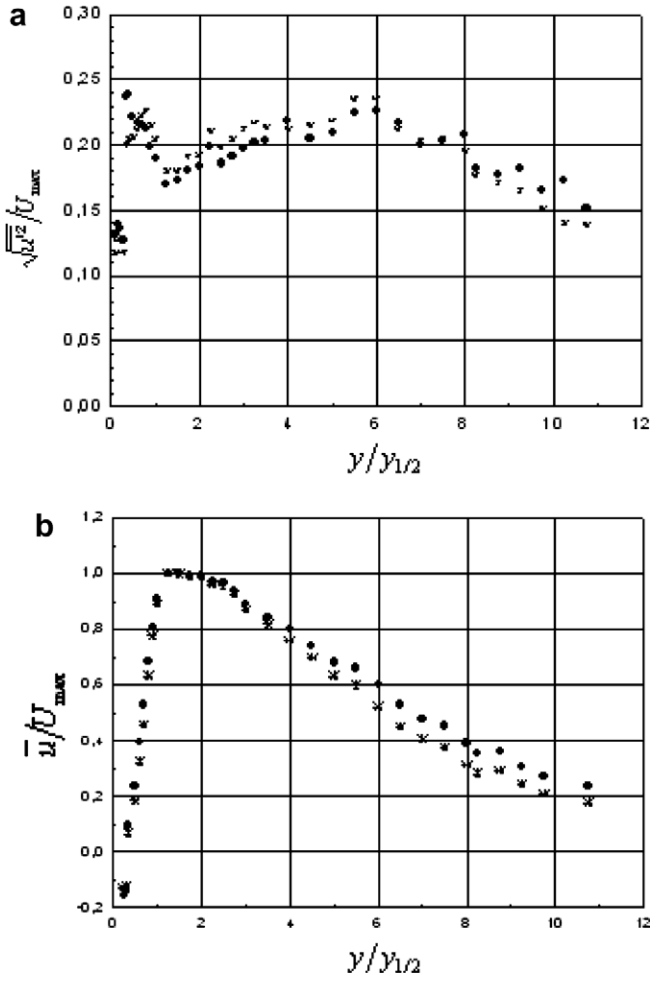

Fig. 4. Example of bias velocity correction on LDA measurements: (a) mean velocity $\bar{u}/U_{max}$; (b) turbulent intensity $\sqrt{\overline{u'^2}}/U_{max}$. Data with velocity bias correction: ●; data without correction: ∗.

the measurement volume used as a weighting factor in the arithmetical averaging procedure. So, a non uniform weighting factor η_i defined by $\eta_i = t_i/\sum_{i=1}^{N} t_i$ (Durao et al., 1980) is introduced, in which t_i is the residence time of the ith particle crossing the measurement volume.

We present in the Fig. 4 an example of the results obtained using the weighted method for the turbulent intensity $\sqrt{\overline{u'2}}/U_{max}$ and for the mean velocity $\bar{u}/U_{max}$. In these profiles, we only present the measured points for which the number of samples exceeds 3000.

In both the external and internal regions, it appears that the uncertainty can reach 30%. Nevertheless, in a numerical analysis done by Zhang (1994), it is mentioned that the velocity bias is lower when the flow fluctuations are three-dimensional and the author concluded that the bias correction is only applicable for flows with $T_u > 30\%$. The method is based on two important assumptions: firstly, the particle distribution in the flow must be homogeneous and secondly, the flow has to be statistically uniform throughout the measurement volume (i.e. no appreciable velocity gradient within the measurement volume). These assumptions cannot be satisfied in particular in the internal zone of the flow. So, we preferred to present all experimental results without correction.

2.3. Characterization of the incoming flow

Preliminary measurements have been made to get a global characterization of the incoming flow at different test sections upstream the step in order to examine the turbulent wall jet development. The flow being assumed two-dimensional, all the measurements were made in the vertical midplane. The two-dimensionality hypothesis was checked by measuring the spanwise distribution of the streamwise velocity upstream of the step and verifying that its distribution is almost uniform in the midplane region. Near the inlet region, measurements of streamwise and spanwise velocity components were performed in the section $x = -17h$ and are reported in Fig. 6. Fig. 5 presents the normalized shear stress $\overline{u'w'}/U_{max}^2$ and the spanwise mean velocity $\bar{w}/U_{max}$ plotted versus $y/y_{1/2}$. The wall jet width $y_{1/2}$ is defined as the distance to the wall of the point where $U(y_{1/2}) = 0.5U_{max}$ in the outer boundary of the jet. We can be confident on the two-dimensionality of the incoming flow upstream of the step considering the small values found for these two quantities. In Fig. 6, the normalized mean streamwise velocity $\bar{u}/U_{max}$ is plotted versus $y/y_{1/2}$ and are in good agreement with the results obtained by Eriksson et al. (1998) in a two-dimensional fully developed turbulent wall jet. In the same Fig. 6, the normal mean velocity profile $\bar{v}/U_{max}$ is presented, obtained as a consequence of the continuity equation by integrating the interpolated streamwise mean velocity profile.

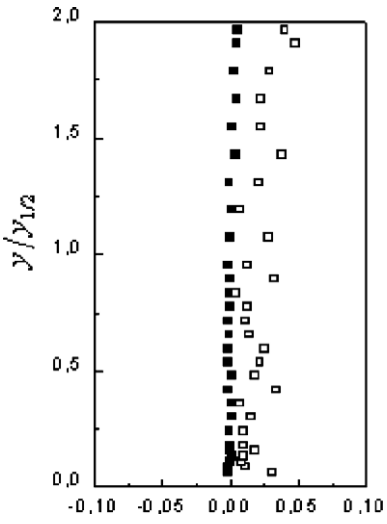

Fig. 5. Normal evolution at $x/h = -17$ of the transverse quantities: ■ : $\bar{w}/U_{max}$, □: $\overline{u'w'}/U_{max}^2$.

2.4. Flow field measurements downstream the step

The recirculation zone which develops near the wall downstream the step is an important flow region, for which much attention has been devoted in the present work. So, the mean and turbulent flow fields are investigated at different cross sections in order to get the streamwise evolution of the turbulent field.

2.4.1. The mean flow structure

A first analysis of the flow in the recirculating and reattachment zones has been previously done by Badri Kusuma (1993). The visualization map, he has obtained, is shown in Fig. 8.

The streamlines predicted numerically (Fig. 10) are in good agreement with these visualizations and these results will be discussed more extensively in the next paragraph. A main recirculating loop is clearly apparent in the visualization and a secondary recirculation bubble also appears close to the step corner.

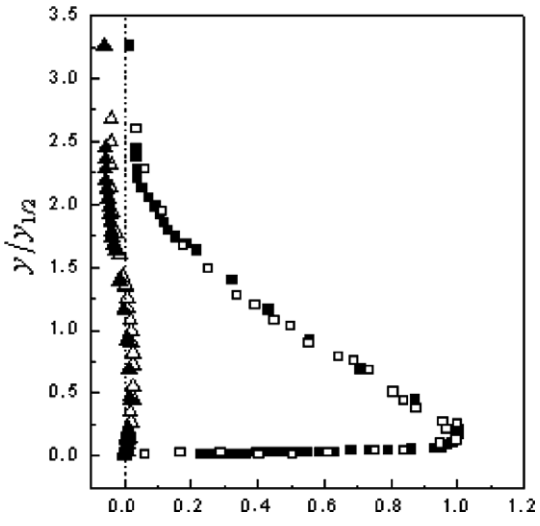

Fig. 6. Mean velocity profiles upstream the step ($x/h = -17$) $\bar{u}/U_{max}$: (■) present LDA measurements; (□) Erickson measurements $\bar{v}/U_{max}$; (▲) present LDA measurements; (△) Erickson measurements.

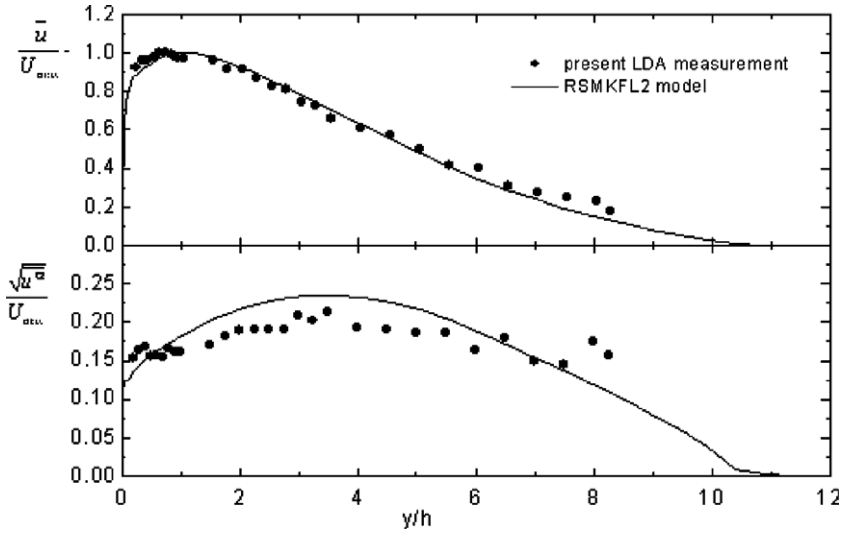

Fig. 7. Evolution of longitudinal mean velocity $\bar{u}/U_{max}$ and turbulent intensity $\sqrt{\overline{u'^2}}/U_{max}$ at $x/h = -5$.

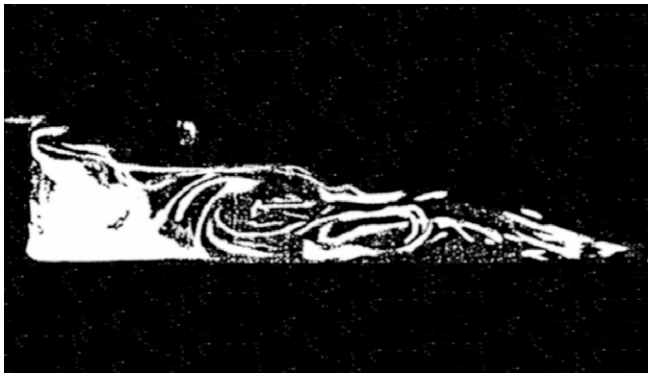

Fig. 8. Laser tomography photo of recirculation flow structure (Badri Kusuma, 1993); zones 3 and 4.

The reattachment point corresponds to the location where the streamline originating at the step edge impinges the wall. Because measurements were not possible very close to the wall, the mean reattachment length could not be obtained very accurately. We can however approximate the reattachment length as between 3, 5*h* and 4*h*.

2.4.2. Spectral analysis

An alternative description of the turbulent flow field has been obtained using a frequency analysis of the flow instead of measuring the correlation functions. This approach allows a detailed picture of the energy distribution among eddies of different sizes.

To calculate the spectral functions, various algorithms can be used, but most of them are requiring uniformly distributed data in time. However, the velocity samples from the LDA measurement system are randomly distributed. Some particular techniques have been proposed for the LDA power spectral analysis (Benedict et al., 1998; Muller et al., 1994) to overcome this problem. In the present study, we used the first order interpolation criterion to rebuild the required data set. It can be shown that the linear interpolation has a slightly lower bias error than the sample and hold technique (Benedict et al., 1998).

In Fig. 9, we present the evolution, at different cross sections, of the energy spectrum. It appears essentially that the equilibrium range is rather inexistent in the region $y/h < 1$. Elsewhere, the spectrum shape is evolving in the vertical direction. This is probably due to the non-homogeneity of the turbulence field and to the hybrid character of the flow resulting from the interaction of two different types of shear. Outside the recirculation zone and for $y/h > 1$, an inertial law is more apparent in the frequency range [10, 100] Hz.

Classical single point closures cannot take into account the non-equilibrium effects due to departures from the standard Kolmogorov energy spectrum. The different plots, given in Fig. 9, show the importance of these departures from equilibrium and justify the use of split spectrum models. The value of f_c shown in these plots, corresponds to the frequency beyond which the noise level, due the interpolation, increases (Adrian and Yao, 1987).

3. Equations and numerical method

3.1. Assumptions at inlet

The fluid flow configuration presented in Fig. 3 corresponds to an incompressible jet issuing from an elongated rectangular nozzle and discharging tangentially on a horizontal flat plate into a uniform stagnant environment. The inlet conditions for the calculation are taken away from the nozzle in a downstream region where the flow is already fully developed. Moreover the flow is considered as steady in the mean.

3.2. Mean flow equations

First, dimensionless variables are introduced with the following definitions:

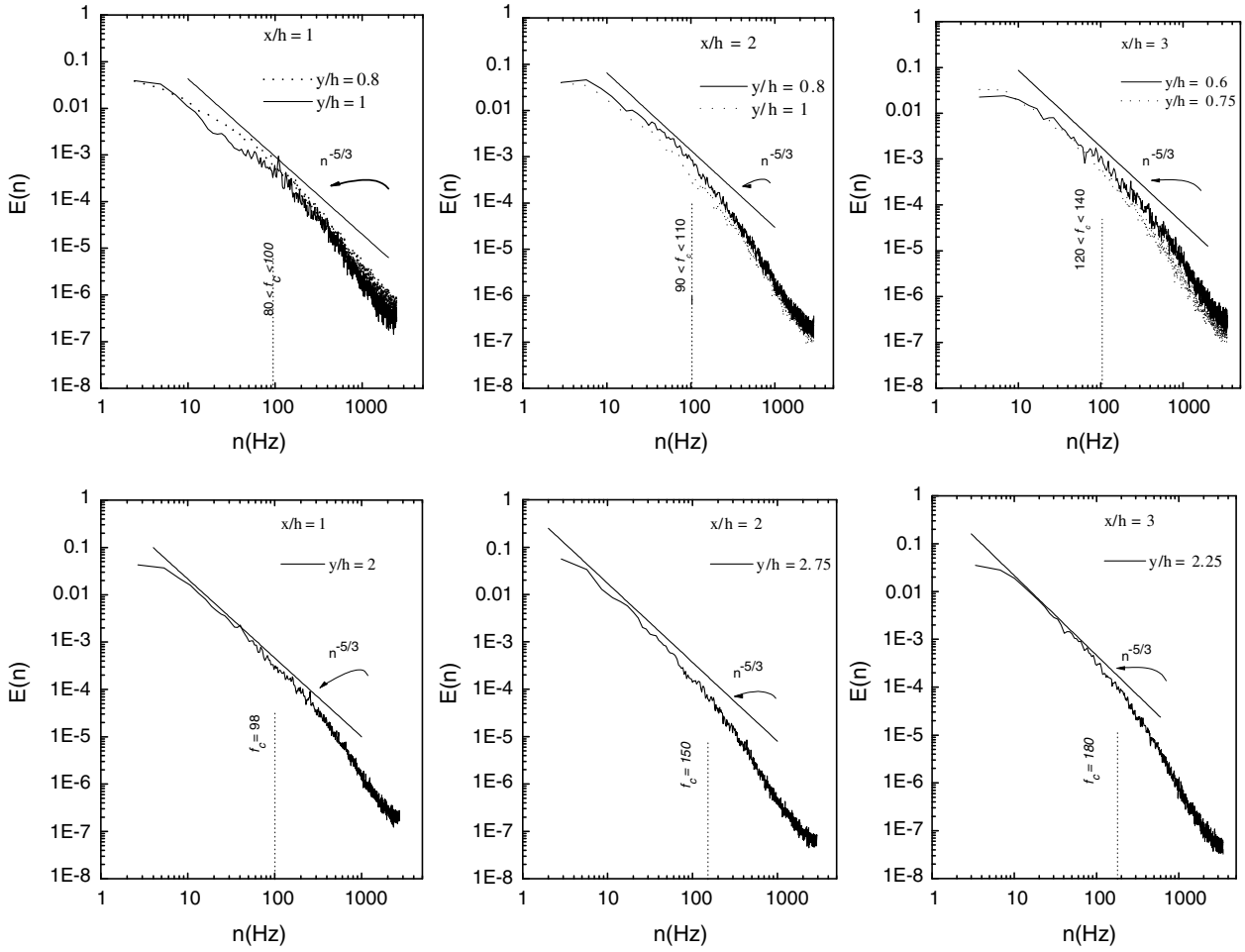

Fig. 9. Evolution of the energy spectrum downstream the step at different streamwise sections: (a) $y/h \leqslant 1$; (b) $y/h > 1$.

$$[x_i] = \frac{x_i}{h}, \quad [x_j] = \frac{x_j}{h}, \quad [\overline{u_i}] = \frac{\overline{u_i}}{U_0}, \quad [\overline{u_j}] = \frac{\overline{u_j}}{U_0}, \quad [k] = \frac{k}{U_0^2}, \quad [\varepsilon] = \frac{\varepsilon h}{U_0^3}, \quad [p] = \frac{p}{\rho U_0^2}, \quad [\overline{u_i u_j}] = \frac{\overline{u_i' u_j'}}{U_0^2}, \quad [\nu] = \frac{1}{Re_h}$$

In the remainder of the paper, we shall disregard the use of square brackets for dimensionless quantities. However, the variables appearing in the legends of some graphs will still be dimensional.

The governing equations for the mean velocity field are given as follows:

1 – Continuity equation:

$$\frac{\partial \overline{u}_i}{\partial x_i} = 0$$

2 – Momentum balance equation:

$$\overline{u}_j \frac{\partial \overline{u}_i}{\partial x_j} = \frac{\partial}{\partial x_j}\left(\nu \frac{\partial \overline{u}_i}{\partial x_j} - \overline{u_i u_j}\right) - \frac{\partial p}{\partial x_i}$$

In this latter equation, the Reynolds stresses need to be modelled using the stress transport model described in the next paragraph.

3.3. Numerical modelling

In such a configuration, including separation and reattachment phenomena, the spectral equilibrium hypothesis would be questionable (see Section 2.4). So, we have been led to use a multiscale approach in the present numerical prediction. The underlying ideas in this approach are extensively commented in Schiestel (1986) and Schiestel (2001) and have been used in various flow configurations (Hanjalic et al., 1980; Garino, 1988; Mataoui, 2002; Gleize, 1994). Multiple scale modelling allows to take into account the fact that turbulence is characterized by a wide spectrum of fluctuations, the different turbulent interactions are then associated with different parts of the evolving spectrum.

The Reynolds stresses components are obtained from the numerical solution of a low Reynolds number second order full stress transport closure (RSM) derived from Launder and Tselepidakis model (1991) and coupled to the two-scale energy-flux model (RSMKFL2).

The two-scale energy-flux model is based on a simplified split spectrum scheme using three spectral zones: production zone, transfer zone and dissipation zone(Schiestel, 1992, 2001) delimited by the wavenumbers κ_1 and κ_2. The $[0,\kappa_1]$ interval corresponds to the wavenumber region in which the main shear production is active, while the $[\kappa_1,\kappa_2]$ wavenumber interval corresponds to the energy cascade transfer zone and then the viscous dissipation zone $[\kappa_2,\infty]$ follows. Energy is transferred out of the first region (production zone) at the rate ε_1 and injected into the transfer zone. Then, the energy is leaving the transfer zone with some delay at a rate ε_2 and is transferred towards the dissipation zone in which it is dissipated at a rate ε. The hypothesis that the dissipation zone contains no appreciable energy allows to suppose $\varepsilon=\varepsilon_2$. In the usual single point closures, there is no recognition of the changes in shape of the energy spectrum, so that $F^{(1)}=F^{(2)}=\varepsilon$.

To characterize the portioning of the spectrum, two parameters can be defined $\zeta=k^{(1)}/k^{(2)}$ and $\theta=F^{(1)}/F^{(2)}$. The first one ζ describes the shape of the energy spectrum: it allows to distinguish a spectral energy distribution having a bump in the production range from an energy distribution having a bump in the smaller scale range. The parameter θ characterizes the degree of spectral imbalance. The evolution of the energy spectrum, at different cross sections inside the recirculation zone presented in Fig. 9 shows that standard equilibrium distributions are not obtained in this region.

The multiple scale model allows to mimic the cascade process by solving partial turbulence kinetic transport equations. The energy flux $F^{(1)}$ out of the production zone is directly influenced by mean strain, while the flux $F^{(2)}$ is not directly dependent on the mean strain. The dissipation is then coupled with the mean flow with a time delay due to the spectral pipeline.

Using tensor notation, the transport equations for the Reynolds stress transport model coupled to the two-scale energy model are given below:

$$\frac{\mathrm{d}R_{ij}}{\mathrm{d}t}=P_{ij}+\Pi_{ij}+D_{ij}-\varepsilon_{ij} \tag{1}$$

where $P_{ij}=-(R_{ij}U_{j,p}+R_{jp}U_{i,p})$ is the production term, D_{ij} combines the turbulent diffusion D^{T}_{ij} which is interpreted as the diffusion due to both velocity and pressure fluctuations (Daly and Harlow, 1970) and the viscous diffusion D^{v}_{ij} which cannot be neglected in the low Reynolds number region near walls. More precisely: $D^{\mathrm{T}}_{ij}=C_{\mathrm{s}}(\sigma_{\mathrm{pl}}R_{ij,p})_{,l}$ and $D^{v}_{ij}=\nu R_{ij,ss}$ with $\sigma_{\mathrm{pl}}=\frac{k.R_{\mathrm{pl}}}{F^{(1)}}$ and $C_{\mathrm{s}}=0.22$.

The viscous dissipation tensor ε_{ij} has been modelled in order to conform to the wall limits obtained from Taylor series expansions of the fluctuating velocities (Launder and Reynolds, 1983):

$$\varepsilon_{ij}=f_{\mathrm{A}}\varepsilon^{*}_{ij}+(1-f_{\mathrm{A}})\left[f_{\mathrm{s}}\frac{\varepsilon R_{ij}}{k}+\frac{2}{3}(1-f_{\mathrm{s}})\varepsilon\delta_{ij}\right] \tag{2}$$

with f_{A}, f_{s} and ε^{*}_{ij} defined as follows: $f_{\mathrm{s}}=\mathrm{e}^{-Re_t^2/40}$, $f_{\mathrm{A}}=\mathrm{e}^{-20A^2}\mathrm{e}^{-Re_t^2/20}$.

$$\varepsilon^{*}_{ij}=\frac{\varepsilon}{k}\cdot\frac{R_{ij}+R_{im}n_jn_m+R_{jm}n_in_m+R_{ml}n_mn_ln_in_j}{1+\frac{3}{2}\cdot\frac{R_{pq}}{k}n_pn_q}$$

The term Π_{ij} denotes the pressure–strain correlation and can be decomposed, in classical way, into three parts:

$$\Pi_{ij}=\phi^{(1)}_{ij}+\phi^{(2)}_{ij}+\phi^{(w)}_{ij}. \tag{3}$$

The first term $\phi^{(1)}_{ij}$ represents the slow nonlinear return to isotropy and is modelled as a quadratic development in the stress anisotropy tensor, the coefficients being sensitized to the invariants of anisotropy. This term is also damped near the wall:

$$\phi^{(1)}_{ij}=-\left[\tilde{c}_1a_{ij}+c'_1\left(a_{im}a_{mj}-\frac{1}{3}\mathrm{II}\cdot\delta_{ij}\right)\right]\varepsilon \tag{4}$$

The two functions, $\tilde{c}_1=(3.1\sqrt{A\cdot\mathrm{II}}+1)(1-f_{\mathrm{s}})$ and $c'_1=3.72\sqrt{A\cdot\mathrm{II}}(1-f_{\mathrm{s}})$, are deduced from Craft's high Reynolds number proposals (see Craft, 1991; Schiestel, 2006).

In the previous hypotheses, $a_{ij}=\frac{R_{ij}-\frac{2}{3}k\cdot\delta_{ij}}{k}$ denotes the stress anisotropy tensor. Also, $A=1-\frac{9}{8}(\mathrm{II}-\mathrm{III})$ is the Lumley's flatness parameter where II and III are the second and third invariants of anisotropy defined as the traces of the dot products: $\mathrm{II}=a_{ij}a_{ji}$ and $\mathrm{III}=a_{ij}a_{in}a_{jn}$.

The linear rapid part $\phi^{(2)}_{ij}$ includes cubic terms. It can be written as follows:

$$\begin{aligned}\phi^{(2)}_{ij}=&-c_2\left(P_{ij}-\frac{2}{3}P\cdot\delta_{ij}\right)+c_{2c}\varepsilon a_{ij}\frac{P}{\varepsilon}\\&-0.2\left[\frac{R_{mj}R_{li}}{k}(U_{m,l}+U_{l,m})-\frac{R_{lm}}{k}(R_{im}U_{j,l}+R_{jm}U_{i,l})\right]\\&-\min(0.6,A)[\mathrm{II}(P_{ij}-D_{ij})+3a_{mi}a_{nj}(P_{mn}-D_{mn})]\end{aligned} \tag{5}$$

with $c_2=0.6$ and $c_{2c}=c_2$.

The third term ϕ^{w}_{ij} is the wall correction term representing the pressure reflection effects near a wall. The form retained here is the one proposed by Gibson and Launder (1978) with however a smaller value of the numerical coefficient. Moreover, the classical length scale $\frac{k^{3/2}}{\varepsilon}$ is replaced by $\frac{k\sqrt{R_{pq}n_pn_q}}{\varepsilon y}$, which is the characteristic length scale of the fluctuations normal to the wall. The final form is:

$$\phi^{(w)}_{ij}=c'_2\left[\phi^{(2)}_{pm}n_pn_m\delta_{ij}-\frac{3}{2}\phi^{(2)}_{ip}n_pn_j-\frac{3}{2}\phi^{(2)}_{pj}n_pn_i\right]\frac{k\sqrt{R_{pq}n_pn_q}}{\varepsilon y} \tag{6}$$

with $c'_2=0.2$ and where y is defined as the distance of the current point location to the nearest wall.

Contraction of the stress equations leads to the total turbulent energy equation:

$$\frac{\mathrm{d}k}{\mathrm{d}t}=P+C_{\mathrm{s}}(\sigma_{ij}k_{,j})_{,i}-\varepsilon+\nu k_{,jj} \tag{7}$$

where $k=k^{(1)}+k^{(2)}$. The partial energy fluxes are determined from the following transport equations (See Schiestel (2006)):

$$\frac{\mathrm{d}k^{(1)}}{\mathrm{d}t} = P^{(1)} - F^{(1)} + C_{\mathrm{s}}^{(1)}(\sigma_{ij}k_{,j}^{(1)})_{,i} - \varepsilon^{(1)} + \nu k_{,jj}^{(1)} \tag{8}$$

$$\frac{\mathrm{d}k^{(2)}}{\mathrm{d}t} = P^{(2)} + F^{(1)} - F^{(2)} + C_{\mathrm{s}}^{(2)}(\sigma_{ij}k_{,j}^{(2)})_{,i} - \varepsilon^{(2)} + \nu k_{,jj}^{(2)} \tag{9}$$

$$\frac{\mathrm{d}F^{(1)}}{\mathrm{d}t} = C_{F0}^{(1)}\frac{P^{(1)}F^{(1)}}{k^{(1)}} - C_{F2}^{(1)}\frac{F^{(1)^2}}{k^{(1)}} + C_{F3}^{(1)}\left(\sigma_{ij}F_{,j}^{(1)}\right)_{,i} - C_{F4}^{(1)}\frac{F^{(1)}\tilde{\varepsilon}^{(1)}}{k^{(1)}} + \Sigma^{(1)} + \nu F_{jj}^{(1)} \tag{10}$$

$$\frac{\mathrm{d}F^{(2)}}{\mathrm{d}t} = C_{F0}^{(2)}\frac{P^{(2)}F^{(2)}}{k^{(2)}} + C_{F1}^{(2)}\frac{F^{(1)}F^{(2)}}{k^{(2)}} - C_{F2}^{(2)}\frac{F^{(2)^2}}{k^{(2)}} + C_{F3}^{(2)}(\sigma_{ij}F_{,j}^{(2)})_{,i} - C_{F4}^{(1)}\frac{F^{(2)}\tilde{\varepsilon}^{(2)}}{k^{(2)}} + \Sigma^{(2)} + \nu F_{jj}^{(2)} \tag{11}$$

$$\varepsilon = F^{(2)} + \varepsilon^{(1)} + \varepsilon^{(2)} \quad \text{and} \quad P = P^{(1)} + P^{(2)} \tag{12}$$

where $P^{(m)}$ represents the main strain production rate: $P^{(m)} = -R_{ij}^{(m)}U_{i,j}$ $(m = 1, 2)$

One assumes $C_{\mathrm{s}} = C_{\mathrm{s}}^{(1)} = C_{\mathrm{s}}^{(2)}$.

The viscous dissipation $\varepsilon^{(m)}$ is defined as:

$$\varepsilon^{(m)} = \underbrace{\frac{f_T}{1-f_T}F^{(m)}}_{\tilde{\varepsilon}} + 2\nu\sqrt{\frac{k^{(m)}}{k}}\left(\sqrt{k^{(m)}}\right)_{,j}\left(\sqrt{k}\right)_{,j} \quad (m = 1, 2) \tag{13}$$

with $f_T = 0.3\exp(-Re_T^2)$ and $Re_T = \frac{k^2}{\nu\tilde{\varepsilon}}$.

Closure hypotheses on the turbulent anisotropic diffusivities are $\sigma_{pm} = \frac{k.R_{pm}}{F^{(1)}}$ and

$$\Sigma^{(m)} = 2\nu\frac{k^{(m)}}{F^{(1)}}R_{jq}U_{i,jl}U_{i,ql} = 2\nu\frac{k^{(m)}}{F^{(1)}}R_{nn}\left(\frac{\partial^2 U}{\partial n^2}\right)^2 \quad (m = 1, 2) \tag{14}$$

The partial Reynolds stresses can be defined as follows:

$$R_{ij}^{(1)} = \frac{2}{3}k^{(1)}\cdot\delta_{ij} + \alpha^{(1)}\cdot a_{ij} \quad \text{and} \quad R_{ij}^{(2)} = \frac{2}{3}k^{(2)}\cdot\delta_{ij} + \alpha^{(2)}\cdot a_{ij} \text{ verifying } R_{ij} = \frac{2}{3}k\cdot\delta_{ij} + (\alpha^{(1)} + \alpha^{(2)})\cdot a_{ij} \tag{15}$$

where $\alpha^{(1)} = \frac{k}{k^{(1)}+\beta k^{(2)}}\cdot\frac{Re_T}{1+Re_T} + \frac{1}{1+Re_T}$, $\alpha^{(2)} = \frac{\beta k}{k^{(1)}+\beta k^{(2)}}\cdot\frac{Re_T}{1+Re_T} + \frac{1}{1+Re_T}$.

with $\beta \approx 0.1$ or even at a first approximation $\beta = 0$.

3.4. Numerical procedure

The flow is considered as fully turbulent except in the viscous sublayer. The equations for the mean and the turbulent fields are solved as transport equations with convection, diffusion and source terms of the general form:

$$\frac{\partial}{\partial x}(\rho U\phi) + \frac{\partial}{\partial y}(\rho V\phi) - \frac{\partial}{\partial x}\left(\Gamma_\phi\frac{\partial\phi}{\partial x}\right) - \frac{\partial}{\partial y}\left(\Gamma_\phi\frac{\partial\phi}{\partial y}\right) = S_\phi$$

where $\phi = U$, V, R_{ij} and $k^{(1)}$, $k^{(2)}$, $F^{(1)}$, $F^{(2)}$ for the two-scale model.

The coefficients Γ_ϕ and S_ϕ are given explicitly for each variable ϕ.

The equations are discretized using a finite volume technique on staggered meshes with variable space steps. The pressure–velocity coupling is achieved using the SIMPLER algorithm (Patankar, 1980). A power law interpolation scheme is used for the convection–diffusion terms. As usual, the source terms in the turbulence equations are linearized to ensure the stability of the solution. A tri-diagonal matrix algorithm (TDMA) allows the solution of the discretized equations and non-linearities are solved by sub-iterations. For the stress tensor components, an efficient block iterative procedure is used.

Grid independence tests have shown that a grid size (NX = 120, NY = 100) produces satisfactory accuracy. In all the discretization meshes, a refinement has been introduced near each wall to take into account the thin viscous sublayer. On the horizontal wall upstream the step, the first calculation point inside the domain is located at $y^+ \approx 0.013$ (for $x = -5h$). Downstream the step, it is near $y^+ \approx 0.28$ (for $x = +15h$).

The equations for partial quantities $k^{(1)}$, $F^{(1)}$, $k^{(2)}$, $F^{(2)}$ are solved successively in this order and then the total stress equations are solved using the value $k = k^{(1)} + k^{(2)}$ wherever the kinetic energy appears in the equations. It is verified after convergence that the trace R_{jj} obtained from the stress equations goes to exactly to $2k$ obtained from the partial energy equations.

3.5. Boundary conditions

At the inlet of the calculation domain $(x = -15h)$, imposed profiles for mean velocity and turbulence quantities are taken from experimental data in a turbulent wall jet. The turbulent dissipation profile which is not known experimentally, is calculated from $\varepsilon = \alpha\cdot\frac{k^{3/2}}{l_c}$, where $k = (\overline{u'2} + \overline{v'2} + \overline{w'2})/2$, α is a numerical factor and l_c a characteristic length scale of the wall jet chosen as $l_c = y_{1/2}$. Partial energies and fluxes are deduced from an equilibrium hypothesis:

$$k^{(1)} = \frac{3}{4}k, k^{(2)} = \frac{1}{4}k \text{ and } F^{(1)} = F^{(2)} = \varepsilon,$$

On the wall boundaries, all mean and turbulent dynamical quantities are put to zero.

The free outlet boundary conditions for any quantity V, $k^{(1)}$, $k^{(2)}$, R_{ij}, $F^{(1)}$ or $F^{(2)}$ denoted by ϕ are $\frac{\partial\phi}{\partial x} = 0$. The mean pressure is imposed at exit and the U-component of velocity is calculated from the continuity equation.

At the upper free boundary, two cases must be distinguished:

- If the fluid leaves the calculation domain ($V > 0$), then the condition for U, $k^{(1)}$, $k^{(2)}$,R_{ij}, $F^{(1)}$ and $F^{(2)}$ is $\frac{\partial\phi}{\partial y} = 0$ and V is obtained from the continuity equation.
- If the fluid enters the calculation domain ($V < 0$), then free stream quantities are imposed.

3.6. Numerical test

A preliminary computational test has been carried on to appraise the performance of the hybrid stress transport and two-scale energy model (RSMKFL2) in predicting the reattachment length which is one of the most important parameter to control in separation and reattachment phenomena. The results showed that this length is better predicted by the two-scale version of the model, by approximately 10%. The single scale version of the model using standard numerical constants over-predicted this parameter relatively to the experiments.

4. Results and discussion

Preliminary results obtained in the wall jet, both experimentally and numerically, have provided a description of the flow field upstream the backward facing step and have given in particular the precise state of the wall jet immediately prior to separation.

The velocity profiles are presented at an upstream section of the step, $x/h = -5$ (see Fig. 7). We can note a satisfactory agreement between computational and experimental LDA results. Then, in the remainder of the paper, our attention will be mainly focussed on the structure and behaviour of the flow downstream the step. So, all the results presented hereafter relate to this region.

The following paragraph gives an analysis of the data collected from present LDA and HW (Badri Kusuma, 1993) measurements in the separation/reattachment region. The numerical modelling approach is also compared and tested against the available measurements. Let us remark also that the numerical calculation allows to extend the analysis to additional quantities that cannot be directly measured.

4.1. Numerical prediction of the flow structure

Fig. 10 shows the average streamlines map of the mean flow. One can clearly observe the development of two recirculation bubbles. The smaller recirculation bubble is located close to the lower step corner and the main adjacent recirculation bubble is located immediately downstream. The small one is extending approximately $1.0h$ in length in the x-direction and approximately $0.8h$ in the y-direction. The same flow pattern was observed by Schram et al. (2004) in a configuration corresponding to an asymmetrical channel expansion with a 1.25 expansion ratio. It was noted also in their case that the small bubble is counter clockwise and its size is approximately $1.0h$ in the streamwise direction and $0.7h$ in the wall normal direction. The large main bubble is limited above by the separating streamline which runs from the step edge down to the reattachment point. However, a difference between these two experiments is noticed: the large bubble length produced by an incoming wall jet flow is distinctly shorter than the one corresponding to channel flow configuration.

The influence of the expansion ratio E_r on the reattachment length in a channel has been studied by Durst and Tropea (1981) and Ra and Chang (1990). These works have shown that the reattachment length was increasing for larger values of E_r. However, in the present study the expansion ratio E_r cannot be defined clearly, and the explanation that are given seems to be related to another phenomenon. Rather, we are led to suppose that the higher turbulence intensity in the upper free boundary of the incoming wall jet, which is characterized by the dominance of large eddies enhancing turbulent diffusion, might have a shortening effect on the recirculation bubble. The effect of turbulence intensity on shortening the reattachment length is also noticed by Isomoto and Honami (1989).

Numerically, the value of the reattachment length is obtained from the location of the zero friction coefficient. It is found in the present case to be equal to $4.5h$ in the mean. Nevertheless, we must point out that the numerical prediction of the reattachment length depends on the inlet boundary conditions and in particular is very sensitive to the dissipation profile at inlet. If the numerical coefficient α in the viscous dissipation approximation used at inlet is no longer taken equal to unity but rather a value chosen between 0.3 and 0.5, the reattachment length approaches the one obtained experimentally. However, in these conditions, the turbulent quantities in the downstream main flow presents some overshoot compared to the experimental values.

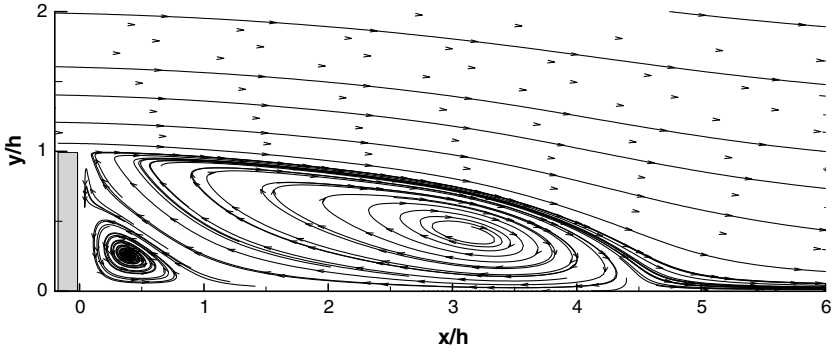

Fig. 10. Numerical prediction of the flow pattern downstream the step (average streamlines of the mean flow).

Departures from equilibrium turbulence may occur when the production is strongly varying in space or when two turbulent fields with differing characteristic scales are interacting. In order to appraise the level of departure from equilibrium in the turbulence field, contour lines of the spectral shape parameter $\xi = k^{(1)}/k^{(2)}$, obtained numerically, are presented in Fig. 11. Practically, this parameter allows distinguishing a spectral energy distribution having a bump in the production range from an energy distribution having a bump in the smaller scales range. The figure shows that the largest values of ξ appear in the vicinity of the reattachment zone where the shear production is high, whereas low values prevail in the recirculation zone. The reference equilibrium values for these parameters are approximately $\xi = 3$ and $\theta = 1$. Indeed, the inlet boundary conditions in the numerical approach were chosen in order to obtain $\xi = 3$ immediately upstream the step.

The next paragraph presents comparisons of the mean velocity and turbulent stress components at several cross sections in which measured data are available. These comparisons are useful for testing the performances of the model.

4.2. Mean flow field

In Fig. 12, we present the evolution of the mean longitudinal velocity profiles at six representative locations within the recirculation region, reattachment and recovery region. Globally, one can consider that a satisfactory agreement between the experimental results and the numerical predictions is achieved. However in the vicinity of the wall, some discrepancies are observed particularly at $x/h = +1$. This particular cross section is probably located at a place where occurs an unsteady behaviour which cannot be captured in

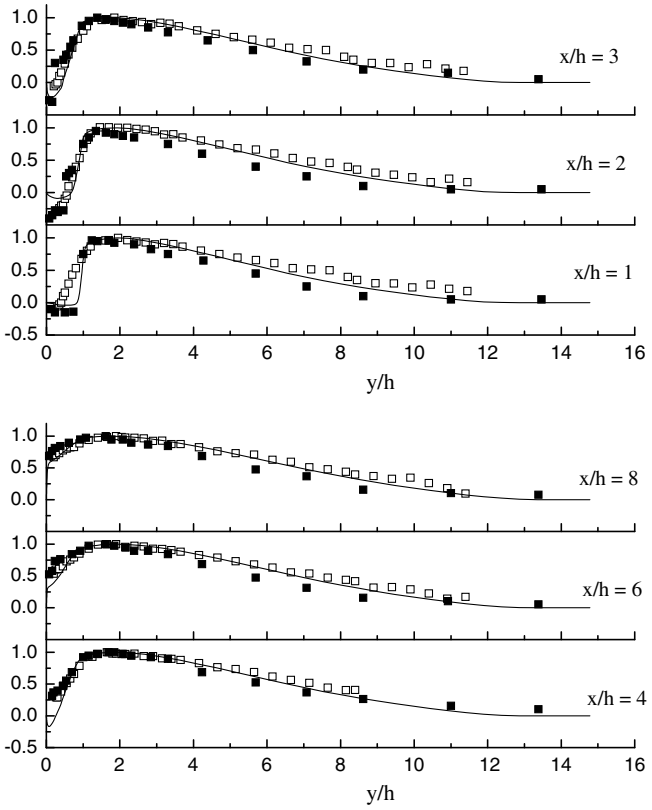

Fig. 12. Longitudinal mean velocity profiles $\bar{u}/U_{max}$ versus $y/y_{1/2}$ at different sections downstream the step present LDA measurements: □; HW measurements (Badri Kusuma, 1993): ■; RSMKFL2 model: —.

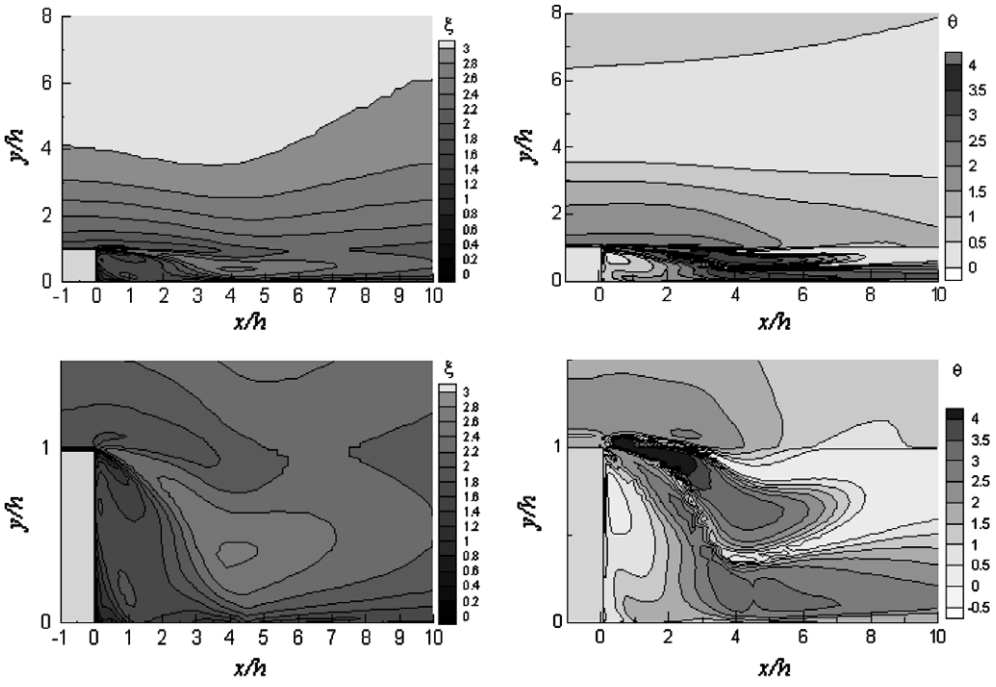

Fig. 11. Contours of spectral shape parameters contours: $\theta = \varepsilon^{(1)}/\varepsilon^{(2)}$ and $\xi = k^{(1)}/k^{(2)}$. (a) Global pattern of the parameters; (b) zoom pattern.

the same manner by the different statistical approaches considered in this work (Hot wire anemometry, Laser Doppler anemometry and statistical second order modelling). Considering the size of the main bubble, approximately $1.0h$ in the streamwise direction and $0.7h$ in the wall normal direction (see also Kostas et al., 2002; Schram et al., 2004), and the interaction mechanism resulting from the breakdown of the shear layer issued from the step edge, this unsteady behaviour should take place close to this section. In addition, the flow in the reattachment zone presents unsteadiness with large scale structures passing through. So, the flapping phenomenon should propagate through the entire recirculation zone. One can suppose then that the oscillation of the large bubble will also affect the small one. Because of volume integration used in the LDA technique, the measurements could be inaccurate in an unsteady zone (a similar deficiency is noted in the reattachment zone close to $x/h = +4$). On the other hand, the analysis of the LDA velocity histograms in this zone shows that the population of seeding particles with positive velocities is more important than the one of negative velocities. This suggests that in the present case, the longitudinal extent of the small bubble exceeds $1.0h$ on an average.

Elsewhere, in the external region $y/h \geqslant +7$, the discrepancies remain moderate, considering the velocity bias we have already mentioned in this region. The best agreement is obtained in the recovery region (after $x/h = 8$).

Fig. 13 shows contour plots of velocity components in the (x, y) plane that illustrate the structure of the flow. The streamwise velocity contours (Fig. 13) show the shear layer issuing from the step edge and reaching the bottom wall near the abscissae $x/h = 4.5$ corresponding to the reattachment point. The negative contours are plotted using dashed lines and the positive contours using solid lines. The negative v contours, noticed in the outer and downstream regions of the reattachment (Fig. 14) all around the recirculation bubble, indicate that most of the flow is directed downward. This must be essentially due to the turbulent activity of the external big eddies towards the wall. In the reattachment region, we can observe also high values in the normal gradient of the v velocity component. Also, we can again notice the two counter-rotating bubbles downstream of the step.

The analysis of the flow structure is consistent with the existence of several sources of turbulence production. Far away from the wall, within the recirculation zone ($x/h < 4$–5), one observes three local maxima in the velocity gradient which induce three main production sources. After the reattachment point ($x/h > 4$ to 5), there are only two, like in the usual case of a tangential wall jet. The definition of the characteristic length l_c (used for instance in the inlet conditions $\varepsilon = \alpha k^{3/2}/l_c$) should take into account these particularities.

In the prediction of the wall characteristics, like skin friction and pressure coefficient, the choice for l_c in the inlet conditions should take into account the turbulent production near the wall in order to reproduce correctly the reattachment length obtained experimentally.

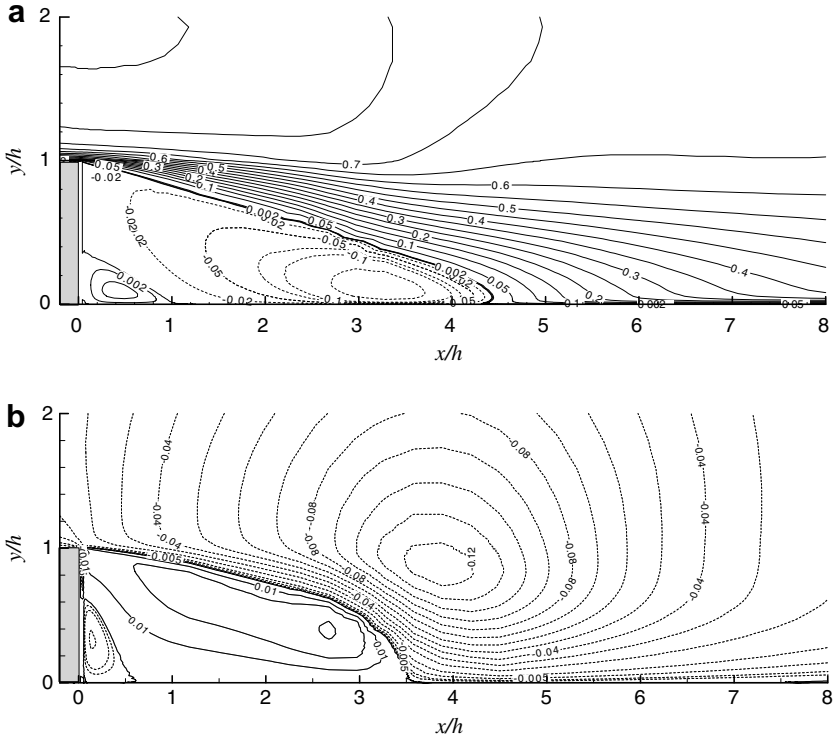

Fig. 13. (a) Numerical contours of the longitudinal velocity component: (—) $\bar{u} > 0$; (– – –) $\bar{u} < 0$; (b) numerical contours of the normal velocity component: (—) $\bar{v} > 0$; (– – –) $\bar{v} < 0$.

4.3. Static wall pressure and skin friction

The two main global characteristics are the pressure coefficient and the friction factor. The static wall pressure coefficient is defined as $C_p = 2\frac{p-p_0}{\rho U^2_{\max}}$ in which the reference pressure p_0 is considered at section $x/h = -10$. The skin friction coefficient is defined as $C_f = 2\frac{\tau_w}{\rho U^2_{\max}}$ in which τ_w denotes the wall shear stress. These coefficients are given in Fig. 14, the two plots show a similar behaviour in particullar in the recirculation region. No experimental result is available for comparison, but we can however say that this behaviour is similar to the one observed in separated boundary layers in the recirculation zone. A significant portion of the pressure rise takes place ahead of the reattachment. Most of the pressure recovery occurs within twice the reattachment length X_r downstream of the step edge. The pressure distribution then becomes asymptotically uniform across the flow.

Concerning the skin friction coefficient distribution, Jovic and Driver (1995) showed that the minimum skin friction coefficient C_{fmin} occurs at approximately a distance $2/3X_r$. In the case of the wall jet configuration, its location is much closer to the reattachment point. The reattachment length can be deduced from interpolation of the calculated skin friction coefficient at the point where $C_f = 0$. The reattachment length X_r obtained from the model is equal to $4.5h$ (with $\alpha = 1$). It is slightly longer than the experimental one which is estimated to reach a value between $3.5h$ and $4h$. Nevertheless, if we consider an inlet dissipation profile hypothesis with a factor $\alpha = 0.4$, it is possible to get a better prediction of the reattachment point located at $x/h = 3.6$. This result is then in good agreement with the experiment.

4.4. Static pressure field

The pressure contours are displayed in Fig. 15. There is a slight negative pressure gradient just prior to the step as indicated by the negative contour lines. Downstream the reattachment point, the pressure gradient remains positive down to approximately $x = 5h$ and then it reverses to an adverse pressure gradient.

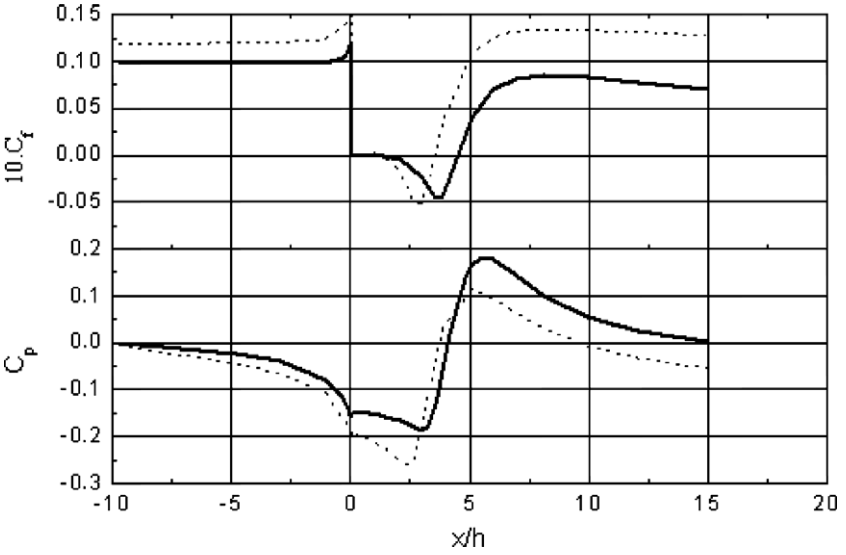

Fig. 14. Skin friction and wall pressure coefficient evolutions downstream the step RSMKL2: (– – –) $\alpha = 0.4$; (—) $\alpha = 1$.

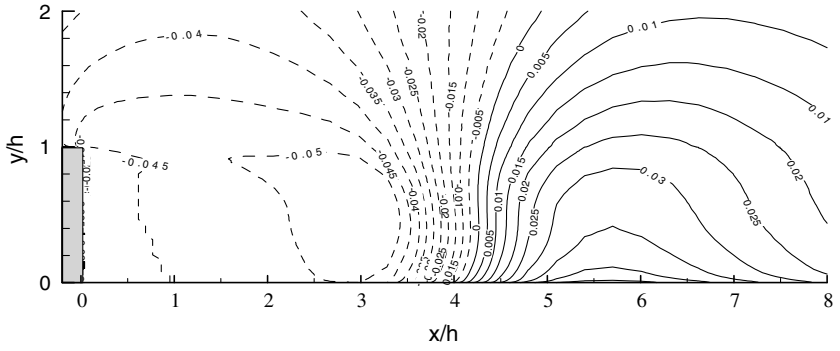

Fig. 15. Contours of mean pressure, (p-p_0) downstream the step: (—) $(p - p_0) > 0$; (– – –) $(p - p_0) < 0$.

4.5. Second order statistical moments

We shall mainly consider the evolution of the longitudinal turbulence intensity and the Reynolds shear stress normalized by the local maximum velocity U_{max}, respectively $\sqrt{\overline{u'2}}/U_{max}$ and $\overline{u'v'}/U^2_{max}$. Fig. 16 shows the streamwise turbulent intensity downstream the step. One can remark that the peak value obtained experimentally in the vicinity of the wall is present but somehow underpredicted by the calculation. In the external region of the wall jet, the numerical prediction of this quantity is in good agreement with the hot wire measurements. We can note also that most of the measurements using laser Doppler anemometry (Karlson et al., 1993b; Schneider et al., 1994) give a significantly higher turbulence level in the outer region of the two-dimensional wall jet than found in the hot wire data. We can conclude thus, that the agreement between LDA and hot wire measurements is questionable in the external zone where high turbulent intensity prevails. Similar differences between hot wire and LDA results have been observed in free jets by Hussein et al. (1994), who concluded that the hot wire measurements are underestimated because of the high local turbulence levels.

The normal Reynolds stress $-\overline{u'v'}$ normalized by U^2_{max} is presented in Fig. 17. In the recirculation zone, the measured values show a large zone with a fairly constant

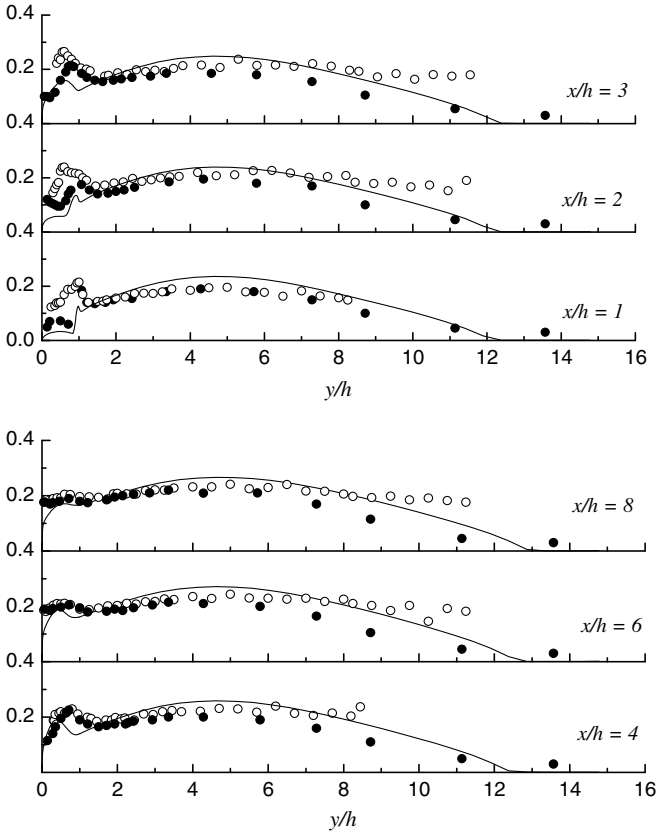

Fig. 16. Evolution of longitudinal turbulent intensity profiles $\sqrt{\overline{u'^2}}/U_{max}$ present LDA measurements: ○; HW measurements: ●; RSMKFL2 model: —.

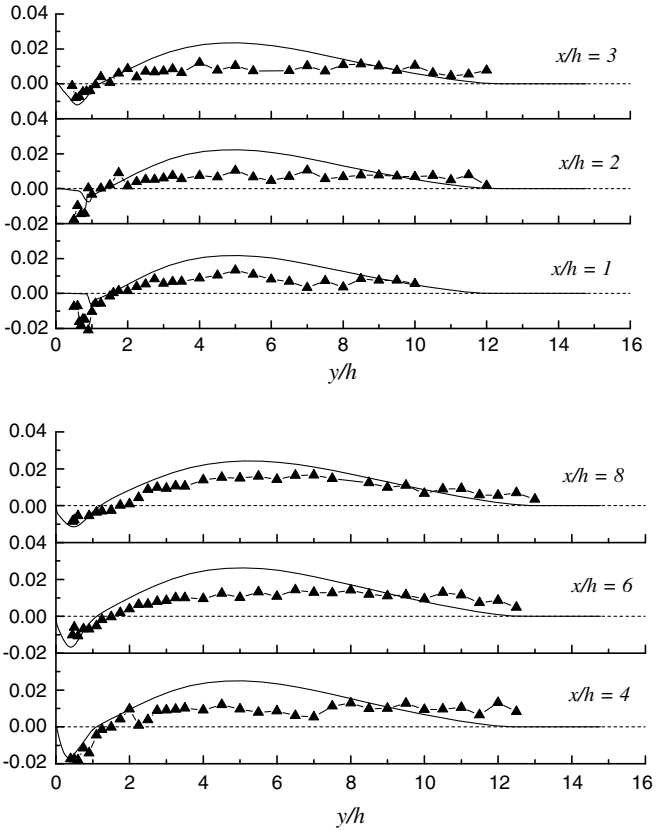

Fig. 17. Profiles of $\overline{u'v'}/U^2_{max}$ downstream the step present LDA measurements: ▲; RSMKFL2 model: —.

behaviour over the flow field. Also, in all this latter region, the model overpredicts this quantity. However, in the recovery region ($x/h \geqslant 6$), the agreement between computational and experimental results becomes better. Further in the recovery zone ($x > 6h$), the Reynolds stress profile tends to reach the usual behaviour of a wall jet profile.

In a wall-jet flow, where the maximum velocity is greater than the external velocity, turbulence produced in the external region diffuses towards the inner one, in contrast with usual boundary-layers or internal flows. The external zone dominated by large energetic eddies influences the step flow, it increases the turbulent diffusion which affect the recirculating region. So, there is a stronger interaction between the different zones of the flow, which induces the flapping phenomenon and the impingement of large structures so that the reattachment length X_r is reduced. These mechanisms can be identified (Fig. 18) from the Reynolds stress evolution. The different sources of turbulent production due to mean shear ($\overline{u'v'} > 0$ with $\partial\overline{u}/\partial y < 0$ in the outer region or in reverse flow and the opposite in the near wall region) located in different regions of the flow, an outer region subjected to intermittency and to the effect of big eddies ($\overline{u'v'} > 0$ with $\partial\overline{u}/\partial y < 0$ also corresponds to a positive eddy rotation) are competing interacting mechanisms. Further downstream in the recovery region, we observe a tendency to relaxation when the effect of the step vanishes progressively after $x/h = 6$. We can note that

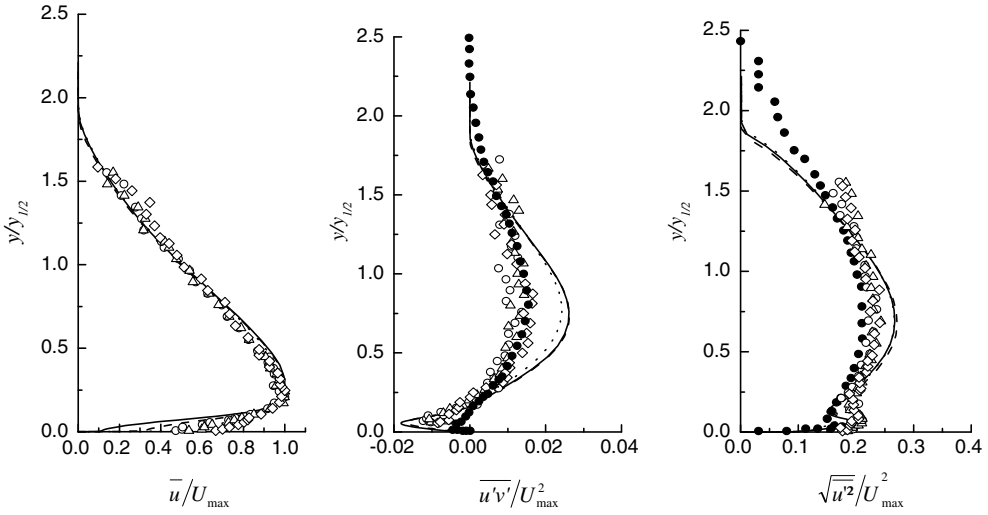

Fig. 18. Profiles of mean velocity and turbulence quantities after the reattachment. present measurements: $x/h = 5$: (○); $x/h = 6$ (△); $x/h = 8$ (♦). Erickson's measurements fully developed turbulent wall jet flow: ●. RSMKFL2 Model: $x/h = 5$: —; $x/h = 6$: – – –; $x/h = 8$: ….

numerical predictions are in good agreement with the experimental results in the recovery zone.

4.6. Relaxation region downstream of reattachment

For studying the approximate self-similarity behaviour of the outer shear layer in the relaxation region ($x > 6h$), the appropriate scaling must be based on global quantities. Profiles of the mean longitudinal velocity and turbulence quantities are normalized on U_{max} and plotted versus $y/y_{1/2}$ in Fig. 18.

Globally, the flow relaxation seems to be very quickly completed in the external region to reach an established state. The effect of the shear layer generated at the step edge, progressively vanishes in the outer region under the activity of the external turbulent structures, but is persisting in the near wall internal region during a longer time. Far away from the reattachment point, the evolution of the experimental profiles is close to the one obtained by Eriksson et al. (1998) in a fully developed wall jet flow.

5. Conclusion

A combined experimental and numerical study was undertaken to analyse a turbulent complex flow. The flow is produced by a tangential turbulent wall jet flowing over a backward facing step. Turbulent eddying zones have been identified, they are controlled by different sources of turbulence: two major shear production sources located on each side of the maximum velocity line and a minor one due to reverse flow inside the recirculation bubble.

In a first stage, measurements of mean and turbulent quantities were carried on and analysed in order to characterize the structure of each flow region and their interactions. The informations deduced from experimental results were sufficient to guide the choice of a numerical prediction model. Once adopted, the numerical approach and its predictions had to be checked against measurements and discuss its performances.

Particularly, we found that the reattachment length is distinctly shorter than the one observed in a usual two-dimensional backward facing step flow (in channel or boundary layer configuration). This early reattachment can be attributed to the additional turbulent diffusive transfer due to the energetic eddying motions in the external flow layer.

The numerical approach is based on one point statistical modelling using a low Reynolds number second order full stress transport closure (after Launder and Tselepidakis model, 1991). As it is well known, a crucial term in the RSM model is the closure of the pressure–strain correlation. This process is important in the overall development of the turbulent flow and may explain the slower growth rate of the plane wall jet compared to a usual free jet. A stress transport model, free from any eddy viscosity assumption, thus seemed adequate for the present problem.

In addition, the transport equations for the Reynolds stresses were coupled to an energy-flux two-scale model based on spectral splitting to account for possible departures from equilibrium. So, the various complexities inherent to this flow (strong anisotropy, nonhomogeneities, multiscale character…) are taken into account in this approach.

The numerical prediction allowed comparisons with experimental data and also to extend the calculation to quantities that are not available experimentally. Globally, we can summarise our results as follows:

- Comparison is satisfactory for the mean and turbulent flow fields except in the external region of the flow where the turbulent intensity is relatively important. This defect has been explained by the effect of large eddies and slow external motion.
- The numerical prediction of the flow pattern in the recirculation zone revealed the existence of two bubbles in

accordance to some previous studies relative to the step flow with a standard boundary layer at inlet.
– Downstream the reattachment point, the flow relaxation is found to get established more quickly in the external region than in the inner one.

We point out that the numerical results are very sensitive to the choice of the characteristic length scale used in the assumption for the inlet dissipation rate profile. It appeared to us that a constant length scale cannot be appropriate to characterize the whole flow including the wall layer and the outer region. It would be probably worthwhile to use different characteristic scales depending on the distance from the wall.

Acknowledgement

The experimental work was carried in the Fluid Mechanics Laboratory (Ecole Centrale de Nantes, UMR 6598, CNRS). We gratefully acknowledge Dr. J.M. Rosant and Dr. P.G. Mestayer for their experimental support.

References

Adams, E.W., Eaton, J.K., 1988. An LDA study of the backward facing step flow including the effects of velocity bias. J. Fluids Eng. 110, 275–282.

Adams, E.W., Johnston, J.P., 1988. Flow structure in the near wall zone of a turbulent separated flow. AIAA J. 26 (8), 932–939.

Adams, E.W., Johnston, J.P., Eaton, J.K., 1984. Experiments on the structure of turbulent reattaching flow. Report MD-43, Thermo Sciences Division, Department of Mechanical Engineering, Stanford University, California.

Adrian, R.J., Yao, C.S., 1987. Power spectra of fluid velocities measured by Laser Doppler Anemometry. Exp. Fluids 5, 17–28.

Badri Kusuma, M.S., 1993. Etude expérimentale d'un écoulement turbulent en aval d'une marche descendante: cas d'un jet pariétal et de la couche limite. Thèse de Diplôme de Doctorat, Ecole Centrale de Nantes.

Badri Kusuma, M.S., Rey, C., Mestayer, P.G., 1992. The effects of wall roughness and external flow structure on backward facing step flows. In: 11th Australasian Fluid Mechanics Conference, Hobart, Australia, pp. 795–798.

Benedict, L.H., Nobach, H., Tropea, C., 1998. Benchmark tests of power spectra from LDA signals. In: Ninth International Symposium on Applications of Laser Techniques to Fluid Mechanics, Lisbon, Portugal.

Bradshaw, P., Wong, F.Y.F., 1972. The reattachment and relaxation of a turbulent shear layer. J. Fluid Mech. 52, 113–135.

Chun, K.B., Sung, H.J., 1996. Control of turbulent separated flow over a backward facing step by local forcing. Exp. Fluids 21, 417–426.

Craft, T.J., 1991. Second-moment modelling of turbulent scalar transport. Ph.D. Thesis, Faculty of Technology, University of Manchester.

Craft, T.J., 1998. Developments in low Reynolds-number second-moment closure and its application to separating and reattaching flows. Int. J. Heat Fluid Flow 19, 541.

Craft, T.J., Launder, B.E., 1996. A Reynolds stress closure designed for complex geometries. Int. J. Heat Fluid Flow 17, 245.

Daly, B.J., Harlow, F.H., 1970. Transport equation in turbulence. Phys. Fluids 13, 2634.

De Brederode, V., Bradshaw, P., 1972. Three-dimensional flow in nominally two-dimensional separation bubbles. I. Flow behind a rearward-facing step. Aero Report 72-19, Imperial College of Science and Technology, London, England.

Driver, D.M., Seegmiller, H.L., 1985. Features of a reattaching turbulent shear layer in divergent channel flow. AIAA J. 23 (2), 163–171.

Durao, D.F.G., Laker, J., Whitelaw, J.H., 1980. Bias Effects in Laser Doppler Anemometry. J. Phys. E: Sci. Instrum. 13, 442–445.

Durst, F., Tropea, C., 1981. Turbulent backward facing step flows in two-dimensional ducts and channels. In: Third International Symposium on Turbulent Shear Flows. University of California, Davis, pp. 18.1–18.5.

Eaton, J.K., Johnston, J.P., 1980. A review of research on subsonic turbulent flow reattachment. AIAA J. 19, 1093–1100.

Eriksson, J.G., Karlson, R.I., Persson, J., 1998. An experimental study of a two-dimensional plane turbulent wall jet. Exp. Fluids 25, 50–60.

Garino, A., 1988. Modélisation d'écoulements turbulents anisotropes à l'aide de schémas multiéchelles aux tensions de Reynolds. Thèse de Diplôme de Doctorat, Univ. d'Aix Marseille II.

Gibson, M., Launder, B.E., 1978. Ground effects on pressure fluctuations in the atmospheric boundary layer. J. Fluid. Mech. 86, 491.

Gleize, V., 1994. Simulation numérique d'écoulements compressibles turbulents hors équilibre à l'aide des schemas multiéchelles, Thèse de Diplôme de Doctorat, Univ. d'Aix Marseille II.

Hanjalic, K., Jakirlic, S., 1998. Contribution towards the second-moment closure modelling of separating turbulent flows. Comput. Fluids 27 (2), 137–156.

Hanjalic, K., Launder, B.E., Schiestel, R., 1980. Multiple time scale concepts in turbulent transport modelling. In: Turbulent Shear Flows II. Second International Symposium on Turbulent Shear Flows. Springer Verlag, pp. 36–49.

Honami, S., Kakajo, I., 1986. A reattaching shear layer to the curved surfaces over a backward facing steps. ASME paper 86-WA/FE-9.

Hussein, H.J., Capp, S.P., George, W.K., 1994. Velocity measurements in a high Reynolds number momentum conserving, axisymmetric turbulent jet. J. Fluid Mech. 258, 31–75.

Isomoto, K., Honami, S., 1989. The effect of inlet turbulence intensity on the reattachment process over a backward facing step. J. Fluid Eng. 111, 87–92.

Johnson, D.A., Brown, D., 1990. A laser Doppler velocimeter approach for near wall three-dimensional turbulence measurements, paper 3.2. In: Fifth International Symposium on Application of Laser Techniques to Fluid Mech, Lisbon, Portugal.

Jovic, S., Driver, D.M., 1994. Backward facing step measurements at low Reynolds number, $Re_h = 5000$, TM 108807, NASA.

Jovic, S., Driver, D.M., 1995. Reynolds number effect on the skin friction in separated flows behind a backward facing step. Exp. Fluids 18 (6), 464–467.

Kang, S., Choi, H., 2002. Suboptimal feedback control of turbulent flow over a backward facing step. J. Fluid Mech. 463, 201–227.

Karlson, R.I., Erikson, J, Persson, J., 1993. An experimental study of a two-dimensional plane turbulent wall jet. Report VU-S 93: B36, Vattenfall Utveckling AB.

Kostas, J., Soria, J., Chong, M.S., 2002. Particule image velocimetry measurements of a backward facing step flow. Exp. Fluids 33, 838–853.

Lasher, W.C., Taulbee, D.B., 1990. Calculation of turbulent backstep flow: commentary on modelling of the pressure strain correlation. In: Rodi, W., Ganic, E.N. (Eds.), Engineering Turbulence Modelling and Experiments 1, vol. 195. Elsevier Science Publishers.

Launder, B.E., Reynolds, W.C., 1983. Asymptotic near-wall stress dissipation rates in a turbulent flow. Phys. Fluids 26 (5), 1157.

Launder, B.E., Rodi, W., 1981. The turbulent wall jets. Prog. Aerospace Sci. 19, 81.

Launder, B.E., Rodi, W., 1983. The turbulent wall jets – measurements and modelling. Ann. Rev. Fluid Mech. 15, 429.

Launder, B.E., Tselepidakis, D.P., 1991. Directions in second moment modelong of near wall turbulence. In: 29th Aerospace Sciences Meeting, January 7–10, Reno, NV, AIAA 91-0219.

Launder, B.E., Reece, G.J., Rodi, W., 1975. Progress in the development of a Reynolds stress turbulence closure. J. Fluid Mech. 78, 537.

Le, H., Moin, P., Kim, J., 1997. Direct numerical simulation of turbulent flow over a backward facing step. J. Fluid Mech. 330, 349–374.

Le Huu Nho, E., 1994. Etude expérimentale de l'écoulement autour d'une marche descendante en dérapage, Thèse de doctorat, IMST, univ. d'Aix Marseille, France.

Lien, F.S., Leschziner, M.A., 1994. Assessment of turbulence transport models including non linear RNG eddy viscosity formulation and second moment closure for flow over a backward–facing step. Comput. Fluids 23, 983–1004.

Mataoui, A., 2002. Modélisation numérique d'un jet plan impactant à l'intérieur d'une cavité de section rectangulaire, Thèse de Doctorat d'état es-Scienses, Univ. des Sciences et Technologie, Alger.

Muller, E., Nobach, H., Tropea, C., 1994. LDA signal reconstitution: application to moment and spectral estimation II. In: Seventh International Symposium on Applications of Laser Techniques to Fluid Mechanics, Lisbon, Portugal.

Nait Bouda, N., Rey, C., Rosant, J., Benabid, T., 2005. Turbulent wall jet interaction with a backward facing step. In: Rodi, W., Mulas, M. (Eds.), ERCOFTAC International Symposium on Engineering Turbulence Modelling and Measurements'6. Elsevier.

Obi, S., Peric, M., Scheuerer, G., 1991. Second-moment calculation procedure for turbulent flows with collocated variable arrangement. AIAA J. 29, 585.

Patankar, S.V., 1980. Numerical heat transfer and fluid flow. McGraw-Hill Book Company.

Ra, S.H., Chang, P.K., 1990. Effects of pressure gradient on reattaching flow downstream of a reaward facing step. Engineering notes. J. Aircraft 27, 93–95.

Schiestel, R., 1986. Multiple-time-scale modelling of turbulent flows in one point closures. Phys. Fluids 30 (3), 722–731.

Schiestel, R., 1992. Les modèles de turbulence à échelles multiples basés sur une partition de spectre, fondements et extensions.

Schiestel, R., 2001. Mécanique des fluides numérique, modélisation statistique de la turbulence et approches multiéchelles, 7ème Ecole de printemps, Aussois 13–19 mai.

Schiestel, R., 2006. Méthodes de modélisation et de simulation des écoulements turbulents. Hermès/Lavoisier, Paris.

Schneider, M.E., Goldstein, R.J., 1994. Laser Doppler measurement of turbulence parameters in two-dimensional plane wall jet. Phys. Fluids 6, 3116–3129.

Schram, C., Rambaud, P., Riethmuller, M.L., 2004. Wavelet based eddy structure eduction from a backward facing step flow investigation using a particle image velocimetry. Exp. Fluids 36, 233–245.

Shuya, Yoshioka, Obi, S., Masuda, S., 2001. Turbulence statistics of periodically perturbed separated flow over backward facing step. Int. J. Heat Fluid Flow 22, 393–401.

Sigurdon, L.W., 1995. The structure and control of a turbulent reattaching flow. J. Fluid Mech. 298, 139–165.

Wygnanski, I., Katz, Y., Horev, E., 1992. On the applicability of various scaling laws to the turbulent wall jet. J. Fluid Mech. 234, 669–690.

Zhang, C.X., 1994. Numerical predictions of turbulent recirculating flows with a k–ε model. J. Wind Eng. Ind. Aerodyn. 51, 177–201.